ПРОГРАММИРОВАНИЕ

MSC 62P10 **DOI: 10.14529/mmp220404**

INTERNAL BONE MARROW DOSIMETRY: THE EFFECT OF THE EXPOSURE DUE TO ^{90}Sr INCORPORATED IN THE ADJACENT BONE SEGMENTS

***A.Yu. Volchkova*[1], *P.A. Sharagin*[1], *E.A. Shishkina*[1,2]**
[1]Urals Research Center for Radiation Medicine, Chelyabinsk, Russian Federation
[2]Chelyabinsk State University, Chelyabinsk, Russian Federation
E-mail: alexa_nice2008@mail.ru, pavel.sharagin.1994@gmail.ru, lena@urcrm.ru

The paper is devoted to dosimetric modelling of the human red bone marrow (RBM) internal exposure due to beta-emitting ^{90}Sr incorporated in spongiosa bone. The dose factor calculation (absorbed dose rate due to unit specific activity of ^{90}Sr) is based on the modelling of radiation transport in segments of the skeleton bones with active hematopoiesis. Segmentation considerably simplifies the modelling, but can lead to an underestimation due to electron emission from the neighboring parts of the bone adjacent to the studied segment. The objective of the study is to determine this cross-fire effect on the absorbed dose in RBM. For this purpose, we analyze the results of the numerical experiment on modelling of dose absorption within the bone segments of various shape and size that were parts of the computational phantoms of skeletons of people of different sex and age. We analyze dose factor dependencies on the area of the spongiosa bone surface and the ratio of weights of bone and RBM. It is found that if the area of the spongiosa surface (SS) > 6 cm^2, then the effect of neighboring bone parts exposure is negligible. For a smaller SS the extension of the linear dimensions of the spongiosa bone by 2 mean electron path lengths results in dose factor increase proportional to the ratio of the extended spongiosa bone surface area to the original one to the power of 0,28. For human computational phantoms, these values are in the range 1,03 – 1,21 and are used as adjustment coefficients for the dose factors. Relative standard uncertainty of the adjustment coefficient is 5%.

Keywords: numerical modelling; computational phantoms; ^{90}Sr; red bone marrow; spongiosa bone.

Terms and Definitions

Spongiosa is a bone fragment that contains a network of bone trabeculas and bone marrow filling the intertrabecular space;

DF is a dose factor to convert specific activity of ^{90}Sr incorporated in the trabecular bone volume into the units of the absorbed dose in RBM, Gy/s per Bq/g;

E is a mean absorbed energy in bone marrow (BM) per unit decay of ^{90}Sr incorporated in the trabecular bone volume, J per Bq/kg;

$\lambda_e(\bar{E})$ is a mean length of the free path in spongiosa of the electron of the combined ^{90}Sr+^{90}Y spectrum with the mean energy $\bar{E}$=0,565 MeV (in continuous slowing down approximation), cm;

$\lambda_e(Q)$ is a maximum length of the free path in spongiosa of the electron of the combined ^{90}Sr+^{90}Y spectrum with the maximum energy Q=2,28 MeV (in continuous slowing down approximation), cm;

BV/TV is a normalized histomorphometric parameter of the bone tissue fraction in spongiosa, rel. units;

m_{BM} is a weight of the bone marrow, g;

m_{TBV} is a weight of the trabecular bone, g;

SS is an area of the spongiosa surface, cm^2;

SPSD is a Stochastic Parametric Skeletal Dosimetry method;

RBM is a red bone marrow;

BM is a bone marrow.

Introduction

Anthropogenic bone-seeking beta-emitters, such as Sr isotopes, can enter the body with food and water as a result of the accidents at the nuclear fuel cycle enterprises. Strontium incorporates into the bone tissues of the skeleton and exposes red bone marrow (RBM). Thus, the dosimetry of bone marrow internal exposure due to Sr isotopes is a crucial problem. In particular, in the middle of the previous century the population residing in the Techa riverside settlements was exposed to ionizing radiation as a result of the releases of liquid radioactive waste into the Techa River (Sr isotopes made up a considerable proportion of the composition of the releases) by the "Mayak" Production Association [1].

Assessment of individual RBM doses due to long-lived ($T_{1/2}$=28,79 years) beta-emitter – ^{90}Sr is of primary importance for dosimetry used in support of epidemiological studies performed for the population of the Urals region [2]. One of the key issues of the RBM dosimetry is dosimetric modelling of the radiation transport in bone structures and energy absorption in RBM. The Monte Carlo method is used to model the radiation transport. It takes into account the probability distribution of electron and photon interaction with elements of chemical composition of the bone and bone marrow with due account of their densities and spatial configuration described by 3-dimensional computational phantoms. Elaboration of computational phantoms of the skeleton is complicated by RBM distribution in a large skeleton volume. Moreover, high probability of emission of low energy electrons of ^{90}Sr beta spectrum ($\bar{E}$=0,196 MeV, Q=0,546 MeV) together with ^{90}Y spectrum ($\bar{E}$=0,934 MeV, Q=2,279 MeV) predetermines the necessity to model spongiosa microstructure with the resolution of about dozens of μm. Consequently, voxel size of the computational phantoms of the whole skeleton and even of single large bones can be huge. Thus, technically it is problematic to create a 3-D model of the whole skeleton. That is why a SPSD (Stochastic Parametric Skeletal Dosimetry) method was proposed [3]. Theoretical grounding of the method was described in the studies [4, 5]. SPSD approach proposes to select certain parts of the skeleton with active hematopoiesis and subdivide them into segments [6]. Segments are selected in such a way that the structure of trabecular bone and thickness of the cortical bone are relatively homogenous within the selected volume. Fig. 1 shows an example of scapula segmentation. RBM is contained mainly along the lateral margin, in articular cavity (glenoid), acromion and coracoid.

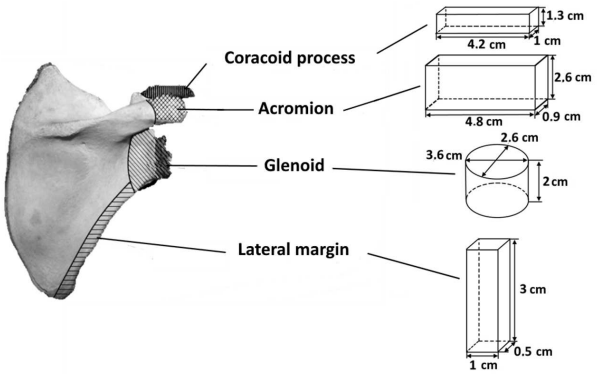

Fig. 1. An example of scapula segmentation into 4 segments with active hematopoiesis and their shape approximation with simple geometric figures. Red bone marrow fraction in other parts of the bone is negligible

Following Fig. 1, segments are approximated by rectangular parallelepipeds and an elliptic cylinder. The height of the parallelepiped describing the lateral margin is less than the corresponding length of the part of the bone and is limited to 3 cm (3 maximum electron

pathlength typical of the ^{90}Sr+^{90}Y decay) [7]. Segments have contact with bone fragments that are not considered. However, bone of these fragments also contain ^{90}Sr isotopes and can contribute to bone marrow exposure in the studied segments. Thus, segmentation can lead to an underestimation of energy absorbed in RBM from the radiation in the adjacent bone areas. The objective of the paper is to evaluate the effect of ^{90}Sr incorporated in the trabecular bone adjacent to the hematopoietic site on RBM dose forming. It is evident that the fraction of energy absorbed in RBM from the adjacent bone depends on the area of contact and the size of the segment. Therefore, to achieve the goal it is necessary to determine the geometric parameters of the segments for which it is necessary to take into account RBM exposure due to neighboring bone parts, and to estimate the value of the adjustment coefficient.

1. Problem Statement

Dose factor is calculated by normalizing the energy absorbed in BM per unit decay of ^{90}Sr (in equilibrium with ^{90}Y) incorporated in trabecular bone according to the equation:

$$DF = E \cdot \frac{m_{TBV}}{m_{BM}}.$$

Following [7], mean length of the electron free path (^{90}Sr+^{90}Y spectrum) in spongiosa ($\lambda_e(\bar{E})$) shortens with the increase in spongiosa density (depends on BV/TV) and can be expressed by the equation:

$$\lambda_e(\bar{E}) = 0,112 + 0,099 \cdot e^{-1,526\frac{BV}{TV}}, (cm).$$

Maximum length of the electron free path in spongiosa $\lambda_e(Q)$ is equal to $5\lambda_e(\bar{E})$. Considering that, in different bones of the skeleton in people of different age, the value BV/TV varies in the range 0,06 – 0,6, then $\lambda_e(\bar{E})$ can take a value from 0,15 to 0,2 cm, and $\lambda_e(Q)$ can take a value from 0,76 to 1 cm [7]. In the volume bounded by the sphere with the radius $\lambda_e(Q)$, the fraction of the energy absorbed in spongiosa from a point source of the electrons makes up 99%. It means that spongiosa with linear dimensions exceeding $\lambda_e(Q)$ absorb 99% of the electron energy of ^{90}Sr+^{90}Y spectrum emitted inside its volume. Dose factors for the segments with linear dimensions exceeding $\lambda_e(Q)$ are insensitive to the variations of shape and size. In other words, a greater part of the emitted energy is absorbed inside the spongiosa volume and radiation losses are negligible.

Consequently, additional radiation from the adjacent parts of the bone has no any contribution of relevance to the total energy absorbed in BM. For the segments with linear dimensions not less than $2\lambda_e(\bar{E})$ dose factors can be considered directly proportionate to the mass ratio $\frac{m_{TBV}}{m_{BM}}$ (or BV/TV), and the influence of the shape and size of the segment can be ignored [7]. However, to avoid underestimating the influence of exposure to the segment from the neighboring areas, let us consider the segments with at least one dimension $< \lambda_e(Q)$. Moreover, we consider the maximum value of $\lambda_e(Q)$ (for minimum bone density), i.e. 1 cm. As a result, linear dimensions of many geometric models turned out to be < 1 cm. Dose factors calculated for such segments can be underestimated and that leads to a biased mean estimate for the skeleton. Therefore, the adjustment coefficient τ is necessary for DF correction. Following [7], absorption of energy in BM depends on the spongiosa density (proportional to BV/TV and bone density), energy losses through the area of the spongiosa surface (SS), and also, probably, on the geometric shape (Sh), see equation (1), where the mass ratio $\frac{m_{TBV}}{m_{BM}}$ is used as a parameter characterizing the spongiosa density.

$$E = f_t\Big(\frac{m_{TBV}}{m_{BM}}, SS, Sh\Big). \quad (1)$$

DF can be expressed by tne non-linear function:

$$DF = f_t\Big(\frac{m_{TBV}}{m_{BM}}, SS, Sh\Big) \cdot \frac{m_{TBV}}{m_{BM}} = F\Big(\frac{m_{TBV}}{m_{BM}}, SS, Sh\Big).$$

The adjustment coefficient can be obtained based on the explicit definition of the function $F\Big(\frac{m_{TBV}}{m_{BM}}, SS, Sh\Big)$ using the data of the numerical experiment (generation of a set of phantoms with different linear dimensions and characteristics of the microstructures) and calculation of the corresponding DF. For the RBM exposure from the neighboring bone areas, the method of adjustment coefficient estimation is based on the calculation of the relative difference between the dose factor of the initial segment (DF_1) and the dose factor (DF_2) obtained with $2\lambda_e(\bar{E})$ extension of the linear dimensions of the initial segment perpendicular to the surface of contact with the neighboring segment, see equation (2).

$$\tau = 1 + \frac{DF_2(SS_2) - DF_1(SS_1)}{DF_1(SS_1)}. \tag{2}$$

In this case, extension of SS_1 (to SS_2) depends on the value of the surface of contact with the neighboring segment.

2. Materials and Methods

2.1. Description of Groups

The segments have at least one linear dimension of the spongiosa $\lambda_e(Q)$. In total 1,695 phantoms were generated. Geometric shape of each segment was described by one of the 3 geometric shapes: rectangular parallelepiped, elliptical cylinder and deformed cylinder (an irregular shaped figure with two parallel elliptical bases and ruled lateral surface). All segments were distributed as follows: 44% are parallelepipeds, 36% are elliptical cylinders, and 20% are deformed cylinders. Other geometric models of bone segments either belong to the large ones, for which the influence of shape and size is negligible, or they are independent objects that do not contact with other bones. Edge lengths of a conditional characteristic box were used for description of spongiosa linear dimensions. If a segment has the shape of a rectangular parallelepiped or elliptical cylinder, then the characteristic box is a circumscribed parallelepiped; if a segment has the shape of a deformed cylinder, then the lengths of the edges of the base of a characteristic box are equal to the mean major and mean minor axes of the upper and lower bases, and the heights of a segment model. All the segments are grouped according to the number of characteristic linear dimensions, $\lambda_e(Q)$: (D1) the group with one linear dimension of the characteristic box (1d) out of the three does not exceed $\lambda_e(Q)$, (D2) the group with two dimensions (2d) out of the three do not exceed the value of $\lambda_e(Q)$, and (D3) for with all three dimensions (3d) are $< \lambda_e(Q)$. Grouping of segments is given in Table 1.

Table 1
Grouping of segments (the name of the group corresponds to the number of characteristic dimensions that are less than maximum length of the pathway)

Group	Dimensions	Number of segments
D1	1d $< \lambda_e(Q)$	843
D2	2d $< \lambda_e(Q)$	696
D3	3d $< \lambda_e(Q)$	156

To validate the correction for the cross firing, we generate separately 24 phantoms with initial linear dimensions and 24 additional phantoms extended by $2\lambda_e(\bar{E})$ relative to the initial models. To create initial phantoms, we use segments with different bone density, different geometric shape (parallelepiped, elliptical cylinder and deformed cylinder) and size. With respect to dimensions, initial phantoms were distributed in the following way: D1 – 7; D2 – 7; D3 – 10 segments.

2.2. Numerical Experiment to Obtain Dose Factors

To calculate mean energy (E) absorbed in BM per unit decay of ^{90}Sr (in equilibrium with ^{90}Y), phantoms of the bone segments generated in the software "Trabecula" were used [11]. Phantoms of the skeleton segments are 3-D voxel models of a simple geometric shape, covered outside with the layer of a cortical bone, and filled with spongiosa inside. The key parameters for the description of the spongiosa are linear dimensions of the geometric figures and fraction of the bone tissue (BV/TV). These parameters were determined by morphological features of the modelled hematopoietic bone sites described in [12, 13]. The volume of BM and bone were calculated in the software "Trabecula".

Absorption of energy in BM was modelled by simulation of the electrons and secondary photons transport with the Monte Carlo method using the MCNP 6.2 code. ^{90}Sr and ^{90}Y radiation spectra were taken from the Java-based Nuclear Data Information System – "Janis 4.1" [14]. ^{90}Sr and ^{90}Y decay was simulated with equal probability (simulating secular equilibrium). The chemical composition of media with radiation transfer was published in [9].

Dose factors were calculated according to [9]. Relative standard uncertainties of dose factors due to shape stylization of the bone segments and bone structures for the phantoms from groups D1, D2 and D3 were evaluated as equal to 15%, 13% and 7%, respectively, within the framework of the study [11]. Voxelization does not result in any significant uncertainty in calculations ($\approx 1\%$).

2.3. Calculation of Spongiosa Surface Area

Spongiosa surface area is calculated for each segment. If the shape of a segment is described by a right-angle parallelepiped with the parameters a, b and h, then the surface area SS_1 is equal to $2(ab + (a + b)h)$.

If the shape of a segment is that of elliptical cylinder, then the surface area SS_2 is equal to $2\pi ab + Lh$ where a and b are semi-axes of the cylinder base, h is the height of a cylinder, L is the length of the arc (perimeter) of an ellipsis. To calculate the perimeter of an ellipsis (L), we use well-known approximation formula (3). The calculation error does not exceed 1%.

$$L \approx 4 \cdot \frac{\pi ab + (a - b)^2}{a + b}. \tag{3}$$

If a segment has the shape of a deformed cylinder, then the spongiosa surface area SS_3 is equal to $\pi(ab + cd) + S_{lateral}$ where a and b are semi-axes of the upper base, c and d are semi-axes of the lower base, $S_{lateral}$ is the surface area of the lateral surface of a cylinder.

The area of the lateral surface of a deformed cylinder is calculated with a numerical method. To do that, the area of a sector corresponding to the 1/4 of a cylinder, was obtained by cross-section of mutually perpendicular planes that pass through the axis of a cylinder. The sector is broken into n parts with an interval $k = 90/n$. The value n is assumed to be equal to 100. For every partition the lateral surface is approximated by a quadrangle. The dimensions of its sides are calculated using the formula of the length of a line segment. The area of a quadrangle S_k with the sides a_k, b_k, c_k, d_k and diagonals e_k and f_k is calculated according to the formula:

$$S_k = \frac{1}{4}\sqrt{4e_k^2 f_k^2 - (b_k^2 + d_k^2 - a_k^2 - c_k^2)^2}.$$

The total area of the lateral surface of a deformed cylinder is calculated according to the formula:

$$SS_{lateral} = 4 \sum_{k=1}^{100} S_k.$$

2.4. Statistical Methods of Analysis of Numerical Experiment Results

Spearman correlation is used to analyze the factors of influence on the dose factor value. Data smoothing with exponential and power functions is performed using the least-square method. Mean value of the module of relative residues expressed as a percentage is used as a measure of data scattering.

Parameters of the function $F\left(\frac{m_{TBV}}{m_{BM}}, SS, Sh\right)$ are defined separately for the 1^{st}, 2^{nd}, and 3^{rd} groups of models ($j = \{D1, D2, D3\}$). The procedure is performed in three steps: 1) define the type of the dependence based on the results of the numerical experiment; 2) select the support function F_{ref} for a specified mass ratio $ref = \frac{m_{TBV}}{m_{BM}}$; 3) adjust the results of the numerical experiment to ref and describe them by a function $F_{aj_{ref}}\left(\frac{m_{TBV}}{m_{BM}}, SS, Sh\right)$. This method allows decreasing the influence of the mass ratio on the data scattering relative to the fitting curve and to refine the parameters of the dependence.

In order to construct a support function, mass ratio is selected by enumerating all the possible variants. To this end, all the data are sorted by mass ratio and sets with similar mass ratios ($n > 7$) are selected in sequence (variation coefficient $< 5\%$ in D1 and $< 3\%$ in D2 and D3). And the range of the SS values in samples should vary by more than 1,5 cm^2.

Power function describing the dependence of the dose factor on mass ratio and SS ($F_{ref,j}$) (variant of a support function) is adjusted for every sample obtained in sequence. In accordance with $F_{ref,j}$ the expected values ($DF_{ref,i,j}$) of dose factors are calculated for every i-th result of the numerical experiment and we derive the ratio $k_{ref,i,j} = \frac{DF_{ref,i,j}}{DF_{i,j}}$ of the expected and the observed ones in the numerical experiment. The scaling function $K_{ref,j}\left(\frac{m_{TBV}}{m_{BM}}\right)$ is obtained by fitting $k_{ref,i,j}$ with exponential function using the least-square method. Further on, scaling function is used as a scaling parameter. Results of the numerical experiment are adjusted to the reference ones as $DF_{aj_{ref,i,j}} = DF_{i,j} \cdot K_{ref,j}\left(\frac{m_{TBV}}{m_{BM}}\right)$. Adjusted values are smoothed with the power function $DF_{aj_{ref,j}}\left(\frac{m_{TBV}}{m_{BM}}, SS\right)$; the power index $b_{ref,j}$ is specified. As a result, in each group j a set of solutions is obtained that corresponds to various ref_j. We take in consideration 50% of the solutions with the highest values of the determination coefficient obtained in scaling function adjustment $K_{ref,j}\left(\frac{m_{TBV}}{m_{KM}}\right)$.

Then we find the intersection of three solution sets (b) that correspond to D1, D2 and D3: $b = b_{D1} \cap b_{D2} \cap b_{D3}$. In the resultant sample, the mean ($\bar{b}$) is estimated. Mean-square deviation from $\bar{b}$ of all the variants of the calculation $b_{ref,j}$ is used as an estimate of standard uncertainty of the parameter $\bar{b}$.

3. Results and Discussion

3.1. Determination of Segment Dimensions that Require Correction for Dose Factor

To perform the analysis, segments are subdivided into three groups in accordance with the number of characteristic parameters exceeding $\lambda_e(Q)$ (Table 1). As it was demonstrated in [9] spongiosa density is the major factor of influence on the dose factor. Fig. 2a and 2b show the dependencies of dose factors on the parameter $\frac{m_{TBV}}{m_{BM}}$ exemplified by D1 and D3 group, respectively.

Data in Fig. 2 are well fitted by an exponential function of the form $y(x) = a(1 - e^{-b \cdot x})$ in all the groups ($R^2 > 0{,}9$). Analysis of the distribution of the relative residues shows

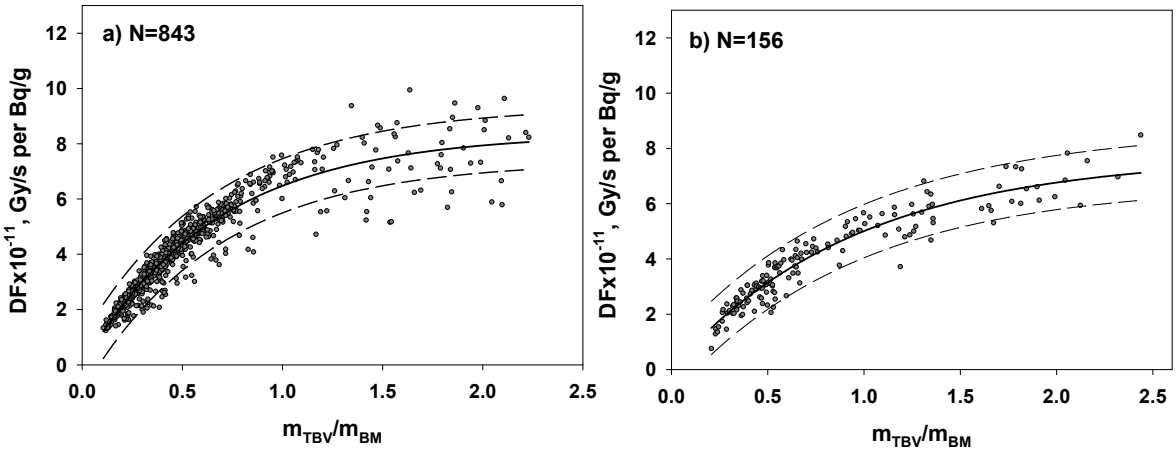

Fig. 2. Dependence of the dose factors on the parameter m_{TBV}/m_{BM} for the group D1 (a) and D3 (b). Solid line shows the fitting line, dashed lines limit the 90% prediction interval. N denotes the number of segments in a group

that mean deviation from the exponential model is 8 – 16%. For large segments (where there is no influence of shape and size) [9] the dependence of dose factors is well described by an exponential growth, but with substantially smaller curvature, and data scattering is on the average ≈5%. In other words, data scattering for small models is significantly wider and is due to a more complex dependence of dose factors on mass ratio than the used approximation, as well as due to other potential factors of influence.

To check the effect of the shape, three types of geometric figures of the computational phantoms are indexed and correlation analysis is performed. No significant correlation between the indices and dose factors in D1 and D2 is found. Weak Spearman correlation is observed for D3 (r=-0,273; p=0,0006). It can be ignored at a first approximation. Note that this conclusion is true only for parallelepiped, cylinder and deformed cylinder. Other figures were not tested. There is no reason to extrapolate the obtained result to any geometry.

Following Fig. 2, the values of dose factors in D3 (SS is in the range 0,23 – 2,97 cm^2) belong to the graph consistently lower than those in D1 (SS is in the range 3,17 – 48,48 cm^2). Dose factors of the second group (SS is in the range 1,01 – 10,85 cm^2) take intermediate values. We can assume multiplicativity of the influence of $SS \times m_{TBV}/m_{BM}$ on the dose factor.

Let us subdivide all the segments into groups according to the values of SS in the following way: 0,2 – 3 cm^2; 3 – 6 cm^2; 6 – 8,3 cm^2; 8,3 – 13 cm^2; 13 – 19,5 cm^2; 19,5 – 48,5 cm^2. Table 2 presents the results of the correlation analysis of dose factors and factors of influence (SS, m_{TBV}/m_{BM}, and $SS \times m_{TBV}/m_{BM}$). As seen from Table 2 the following features are characteristics of segments of each group with the surface area less than 6 cm^2 (they are highlighted in grey in Table 2): 1) r_s for SS is positive and statistically significant ($p < 0{,}05$), and 2) r_s takes a higher value for $SS \times m_{TBV}/m_{BM}$ relative to m_{TBV}/m_{BM}.

In other words, despite weak correlation of dose factors and SS for segments with $SS < 6$ cm^2, the change in the surface area influences the value of the dose factor and the correction for the RBM exposure due to the neighboring areas of the bone can be important. Hence, further when considering the 1^{st}, 2^{nd}, and 3^{rd} groups, the following number of the numerical experiment results are used: 87, 476, and 156, respectively. In the assessment of the dose factor dependence on the spongiosa surface area and taking into account that $\frac{m_{TBV}}{m_{BM}}$ $\left(F\left(\frac{m_{TBV}}{m_{BM}}, SS\right)\right)$, we use the combined parameter $SS \times m_{TBV}/m_{BM}$.

Table 2

Coefficients of Spearman correlation (r_s) between dose factors (DF) and factors of influence

Group	SS(min – max), cm^2	Number of segments	Factors of influence		
			SS	m_{TBV}/m_{BM}	$SS \times m_{TBV}/m_{BM}$
D1	3,17 – 5,99	87	0,232	0,966	0,971
	6,00 – 8,27	135	0,220	0,993	0,985
	8,32 – 12,91	203	−0,0529**	0,977	0,961
	13,01 – 19,49	107	0,0468**	0,981	0,969
	19,5 – 48,48	311	−0,193**	0,954	0,960
D2	1,01 – 6,16	476	0,179	0,878	0,906
	6,17 – 10,85*	220	0,227	0,948	0,950
D3	0,23 – 2,97	156	0,376	0,954	0,965

* There is no enough number of values with $SS > 8{,}3$ cm^2 to single them out into a separate group
** $p > 0{,}05$

3.2. Determination of Correction Coefficient

Let us consider separately three distinguished groups that include only segments with $SS < 6$ cm^2. All the three fitting functions are well described by a power function of the form $y(x) = a \cdot x^b$ ($R^2 > 0{,}87$). Fig. 3 shows an example of dose factor dependence on $SS \times m_{TBV}/m_{BM}$ for D2.

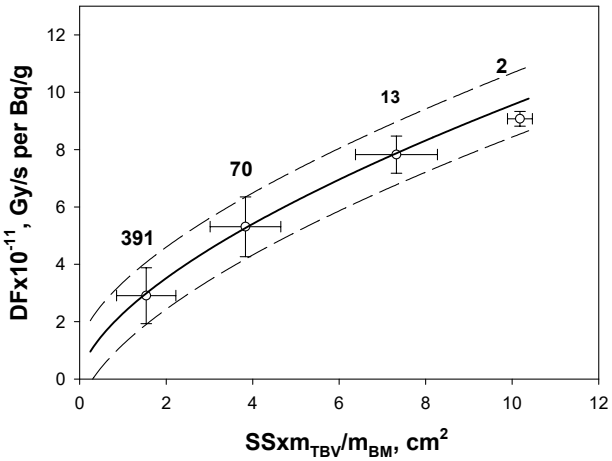

Fig. 3. Dose factor dependence on the combined parameter $SS \times m_{TBV}/m_{BM}$ for D2. Numbers mark the amount of data in the groups; "error bars" correspond to standard deviations. The curve is the power function fitted to non-grouped data, dashed lines limit the 90% prediction interval

For the purpose of illustration, the data in Fig. 3 are combined into groups with the interval 3 cm^2. On the average the scattering of the dose factors relative to the model curve is equal to 14%. For D1 and D3 scattering of the dose factors is 9%.

Taking into account the fact that dose factor dependence on the parameter $SS \times m_{TBV}/m_{BM}$ is of a power mode, we can simplify equation (2) to estimate the correction for the cross firing of the BM due to neighboring parts of the bone:

$$\tau = 1 + \frac{a \cdot \left(SS_2 \times \frac{m_{TBV}}{m_{BM}}\right)^b - a \cdot \left(SS_1 \times \frac{m_{TBV}}{m_{BM}}\right)^b}{a \cdot \left(SS_1 \times \frac{m_{TBV}}{m_{BM}}\right)^b} = \left(\frac{SS_2}{SS_1}\right)^b. \tag{4}$$

In other words, to estimate the correction it is important to estimate exactly the power index b. To do that it is necessary to minimize the data scattering relative to the model.

Variants of the possible reference values are picked out for each of the three sets (D1, D2, and D3) with numerical method by sequential selection of a set of dose factors obtained for the models, where m_{TBV}/m_{BM} can be considered similar (they vary within a narrow range of values). Fig. 4 illustrates the steps of dose factors adjustment exemplified by one of the variants of the reference sample ($m_{TBV}/m_{BM} \in [0{,}49 - 0{,}55]$) from the set D3: 1) construct the variant of a support function F_{ref} (Fig. 4a); 2) construct the scaling function $K_{ref}(m_{TBV}/m_{BM})$ (Fig. 4b) by smoothing $k_i = DF_{ref,i}/DF_i$ with exponent; 3) smooth the adjusted values $DF_{aj_{ref,i}} = DF_i \cdot K_{ref}(m_{TBV}/m_{BM})$ (Fig. 4c) by a power function and determine a power index b.

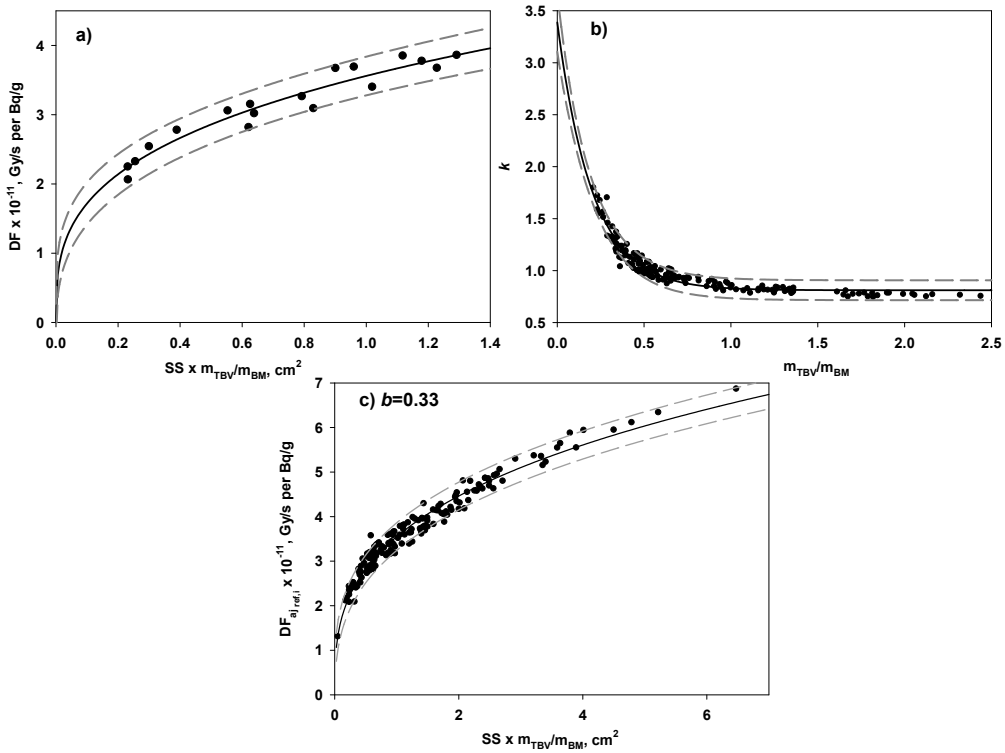

Fig. 4. Example of finding b for the variant of the reference sample (N=18) from the set D3 with $m_{TBV}/m_{BM} \approx 0{,}52$: a) construct the support function; b) construct the scaling function, and c) construct the dependence of the adjusted dose factors on the parameter $SS \times m_{TBV}/m_{BM}$, and estimate the parameter b

Table 3 provides description of the reference samples by groups, support functions, scaling coefficients, as well as adjusted dose factors.

Table 3

Description of the reference samples from the sets D1, D2 and D3, support functions, scaling coefficients, and dependences of the adjusted dose factors on $SS \times m_{TBV}/m_{BM}$ by groups

Characteristics	D1	D2	D3
N of reference samples (elements of sets)	2	17	28
Reference sample size (number of models)	8 – 10	10 – 42	8 – 18
Range of values ref	0,51 – 0,64	0,18 – 0,45	0,35 – 0,56
Support function $F_{ref}(SS \times ref) \times 10^{-11}$, Gy/s per Bq/g	Standart form: $y(SS \times ref) = a \cdot (SS \times ref)^b$		
	R^2: 0,4 – 0,61 a: 3,2 – 3,6 b: 0,26 – 0,27	R^2: 0,2 – 0,32 a: 1,5 – 2,9 b: 0,07 – 0,21	R^2: 0,56 – 0,94 a: 2,8 – 3,7 b: 0,21 – 0,32
Scaling coefficients $K_{ref}(ref)$	Standart form: $y(ref) = a + b \cdot e^{-c \cdot ref}$		
	R^2: 0,87 a: 0,73 – 0,83 b: 2,1 – 2,5 c: 4,1 – 4,2	R^2: 0,73 – 0,77 a: 0,32 – 0,70 b: 1,4 – 2,4 c: 4,4 – 4,6	R^2: 0,92 – 0,94 a: 0,59 – 0,83 b: 2,4 – 3,2 c: 4,86 – 4,95
Adjusted dose factors $DF_{aj_{ref}}(SS \times ref) \times 10^{-11}$, Gy/s per Bq/g	Standart form: $y(SS \times ref) = a \cdot (SS \times ref)^b$		
	R^2: 0,81 – 0,83 a: 3,2 – 3,6 b: 0,27 – 0,28	R^2: 0,50 – 0,70 a: 1,5 – 2,8 b: 0,22 – 0,30	R^2: 0,90 – 0,96 a: 2,8 – 3,7 b: 0,25 – 0,33
Mean scattering of the adjusted dose factors, %	6,2	11,8	4,7

As seen from Table 3, the ranges of the possible values of the power indices b for the adjusted data overlap. As a result of intersection of the sets $b_{D1} \cap b_{D2} \cap b_{D3}$, we obtain the sample that includes 6 variants of the values with the central estimate $\bar{b}$=0,278±0,002 (± standard deviation that corresponds to the error of mean). Standard uncertainty $\sigma(\bar{b})$ is estimated as a mean-square deviation of the combined data of all the possible variants of the reference values and is equal to 0,05.

3.3. Estimating Value of Correction for Cross Firing of BM due to Neighboring Parts of Bone

To estimate the value of correction for cross firing besides knowing the value of b it is necessary to have an idea about the values that the ratio SS_2/SS_1 can take. By extending one of the characteristic parameters of the right-angle parallelepiped after another by two lengths of the free pathway of the electron of ^{90}Sr+^{90}Y spectrum, and by extending the size of the cylinders (both elliptical, and deformed ones) in the direction perpendicular to the bases, we obtain the range of possible ratios SS_2/SS_1 in the studied segments varying in the range 1,1 – 2. It corresponds to the correction coefficients (according to equation (4)) in the range 1,03 – 1,21.

Relative standard uncertainties of the dose factors due to stylization of the shape of the bones and bone structures for the phantoms for D1, D2, and D3 were estimated within

the framework of the study [11] as equal to 15%, 13%, and 7%, respectively. Voxelization does not result in any significant uncertainty in calculations ($\approx 1\%$).

Evidently, it has no sense to use small corrections changing the value of the dose factor by a value comparable to the uncertainty in its estimate. It refers to $SS_2/SS_1 < 1{,}3$ when the predicted correction is $< 7\%$.

Fig. 5 shows the comparison of model predictions with the data obtained with direct calculations for the initial and extended models. It should be noted that the calculation data in Fig. 5 were not used in constructing fitting model and are not viewed as validating ones.

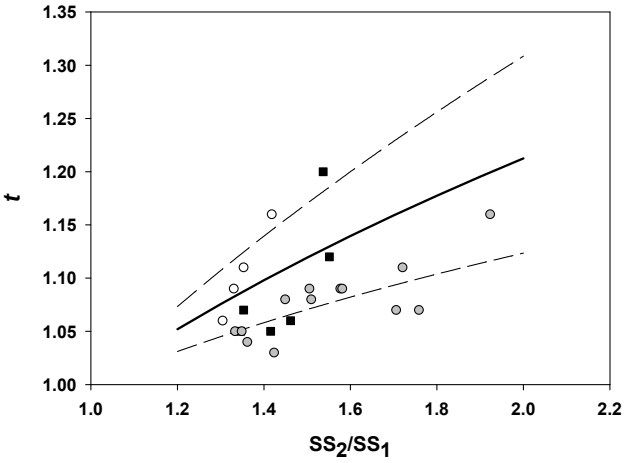

Fig. 5. Comparison of model prediction; solid line denotes dependence of the correction value on SS_2/SS_1 described by a power function; dashed lines limit the 95% prediction interval of the model; dots denote results of the numerical experiment: white circles – D1; black squares – D2; grey circles – D3

Confidence interval of the model predictions is constructed based on the uncertainty of the parameter b. On the average the scattering of the experimental data relative to the model predictions is 4%; maximum deviation does not exceed 9%. It is a good agreement. However, following Fig. 5, the width of the 95% prediction interval of the model is somewhat narrowed and covers only 65% of experimental data. Thus, to estimate correctly the uncertainty of the correction coefficient we can rely on the comparison data of the direct calculations and model predictions, and consider the uncertainty to be equal to relative mean-square deviation, which is 5%.

Conclusion

Correction coefficient is necessary for the segments with the spongiosa surface area < 6 cm^2. It allows to take into account the effect of the RBM exposure due to the neighboring parts of the bone.

Correction coefficient is calculated according to equation (4) with the power index b=0,28. The correction value can vary in the range 1,03 – 1,21. However, if the value of calculated correction is $< 7\%$, which is comparable to the uncertainty of the dose factor itself, then it can be ignored by additionally including the uncertainty of the non-excluded systemic error into the structure of the DF uncertainty.

Relative standard uncertainty of the correction coefficient is 5%.

Acknowledgments. *Financial support of construction of the computational phantoms and Monte Carlo simulations was provided by the Russian Health Studies Program of the U.S. Department of Energy (DOE) under the auspices of the Joint Coordinating Committee for Radiation Effects Research Project 1.1, Techa River Population Dosimetry. Method improvement was funded by the Federal Target Program "Ensuring nuclear and radiation safety".*

References

1. Loke K.S., Padhy A.K., Ng D.C., Goh A.S, Divgi C. Dosimetric Considerations in Radioimmunotherapy and Systemic Radionuclide Therapies: A Review. *World Journal of Nuclear Medicine*, 2011, vol. 10, no. 2, pp. 122–138. DOI: 10.4103/1450-1147.89780
2. Degteva M.O., Shagina N.B., Vorobyova M.I., Shishkina E.A., Tolstykh E.I., Akleev A.V. Contemporary Understanding of Radioactive Contamination of the Techa River in 1949–1956. *Radiation Biology. Radioecology*, 2016, vol. 56, no. 5, pp. 523–534. (in Russian)
3. Degteva M.O., Tolstykh E.I., Shishkina E.A., Shagina N.B., Volchkova A.Yu., Bougrov N.G., Napier B.A., Smith M.A., Anspaugh L.R. Enhancements in the Techa River Dosimetry System: TRDS-2016D Code for Reconstruction of Deterministic Estimates of Dose from Environmental Exposures. *Health Physics*, 2019, vol. 117, no. 4, pp. 378–387. DOI: 10.1097/HP.0000000000001067
4. Degteva M.O., Shishkina E.A., Tolstykh E.I., Zalyapin V.I., Sharagin P.A., Smith M.A., Napier B.A. Methodological Approach to Development of Dosimetric Models of the Human Skeleton for Beta-emitting Radionuclides. *Radiation Hygiene*, 2019, vol. 12, no. 2, pp. 66–75. DOI:10.21514/1998-426X-2019-12-2-66-75 (in Russian)
5. Degteva M.O., Tolstykh E.I., Shishkina E.A., Sharagin P.A., Zalyapin V.I., Volchkova A.Yu., Smith M.A., Napier B.A. Stochastic Parametric Skeletal Dosimetry Model for Humans: General Approach and Application to Active Marrow Exposure from Bone-Seeking Beta-Particle Emitters. *PLos One*, 2021, vol. 16, no. 10, article ID: e0257605, 32 p. DOI: 10.1371/journal.pone.0257605
6. Shishkina E.A., Zalyapin V.I., Timofeev Yu.S., Degteva M.O., Smith M.A., Napier B.A. Parametric Stochastic Model of Bone Structures to be Used in Computational Dosimetric Phantoms of Human Skeleton. *Radiation and Applications*, 2018, vol. 3, no. 2, pp. 133–137. DOI: 10.21175/RadJ.2018.02.022
7. Zalyapin V.I., Timofeev Yu.S., Shishkina E.A. Parametric Stochastic Model of Bone Geometry. *Bulletin of the South Ural State University. Series: Mathematical Modelling, Programming and Computer Software*, 2018, vol. 11, no. 2, pp. 44–57. DOI: 10.14529/mmp180204
8. Sharagin P.A., Shishkina E.A., Tolstykh E.I., Volchkova A.Yu., Smith M.A., Degteva M.O. Segmentation of Hematopoietic Sites of Human Skeleton for Calculations of Dose to Active Marrow Exposed to Bone-seeking Radionuclides. *Medical Physics*, 2018, vol. 3, pp. 154–158. DOI: 10.21175/RadProc.2018.33
9. Shishkina E.A., Sharagin P.A., Volchkova A.Yu. Analytical Description of the Dose Formation in Bone Marrow due to ^{90}Sr Incorporated in Calcified Tissues. *Radiation Safety Issues*, 2021, no. 3, pp. 72–82. (in Russian)
10. ICRP, 1995. Basic Anatomical and Physiological Data for Use in Radiological Protection – The Skeleton. ICRP Publication 70. *Annals of the ICRP*, 1995, vol. 25, no. 2, pp. 1–80.
11. Shishkina E.A., Timofeev Y.S., Volchkova A.Y., Sharagin P.A., Zalyapin V.I., Degteva M.O., Smith M.A., Napier B.A. Trabecula: A Random Generator of Computational Phantoms for Bone Marrow Dosimetry. *Health Physics*, 2020, vol. 118, no. 1, pp. 53–59. DOI: 10.1097/HP.0000000000001127

12. Sharagin P.A., Tolstykh E.I., Shishkina E.A., Napier B.A., Smith M.A., Degteva M.O. Dosimetric Modeling of Bone for Bone-Seeking Beta-Emitting Radionuclides: Size Parameters and Segmentation. *Contemporary Issues of Radiobiology – 2021: International Scientific Conference Proceedings*, Minsk, 2021, pp. 200–203. (in Russian)
13. Tolstykh E.I., Sharagin P.A., Shishkina E.A., Degteva M.O., Napier B.A., Smith M.A. Dosimetric Modeling of Red Bone Marrow Exposure from ^{89,90}Sr: Resolving Age-Dependent Trabecular Bone Parameters. *Contemporary Issues of Radiobiology – 2021: International Scientific Conference Proceedings*, Minsk, 2021, pp. 176–179. (in Russian)
14. Soppera N., Bossant M., Dupont E. JANIS 4: An Improved Version of the NEA Java-based Nuclear Data Information System. *Nuclear Data Sheets*, 2014, vol. 120, pp. 294–296. DOI: 10.1016/j.nds.2014.07.071

Received February 14, 2022

УДК 623.454.862 **DOI: 10.14529/mmp220404**

ДОЗИМЕТРИЯ ВНУТРЕННЕГО ОБЛУЧЕНИЯ КОСТНОГО МОЗГА: ВЛИЯНИЕ ИЗЛУЧЕНИЯ ^{90}Sr, ИНКОРПОРИРОВАННОГО В ПРИЛЕГАЮЩИХ КОСТНЫХ СЕГМЕНТАХ

***А.Ю. Волчкова*[1], *П.А. Шарагин*[1], *Е.А. Шишкина*[1,2]**
[1]ФГБУН Уральский научно-практический центр радиационной медицины ФМБА России, г. Челябинск, Российская Федерация
[2]Челябинский государственный университет, г. Челябинск, Российская Федерация

Настоящая работа посвящена дозиметрическому моделированию внутреннего облучения красного костного мозга (ККМ) человека от бета-излучателя ^{90}Sr, инкорпорированного в губчатой кости. Расчет дозового коэффициента (мощности поглощенной дозы от единичной удельной активности ^{90}Sr) основан на моделировании транспорта излучений в сегментах костей скелета с активным гемопоэзом. Сегментация существенно упрощает моделирование, но может приводить к занижению результатов из-за эмиссии электронов от соседних, прилегающих к рассматриваемому сегменту, участков кости. Целью настоящего исследования является определение влияния перекрестного облучения от соседних участков кости на поглощенную дозу в ККМ. Для этой цели были проанализированы результаты численного эксперимента по моделированию дозообразования в костных сегментах разных форм и размеров, которые входили в вычислительные фантомы скелетов людей разного пола и возраста. Были проанализированы зависимости дозовых коэффициентов от площади поверхности губчатой кости и соотношения масс костной ткани и ККМ. Найдено, что если площадь поверхности губчатой кости (SS) > 6 см^2, то эффект облучения соседними участками кости пренебрежимо мал. Для меньшей SS приращение линейных размеров губчатой кости на 2 средние длины свободного пробега электронов приводит к увеличению дозового коэффициента пропорционально отношению увеличенной площади поверхности губчатой кости к исходной в степени 0,28. Для вычислительных фантомов человека эти значения варьируют от 1,03 до 1,21 и могут быть использованы как поправочные коэффициенты для дозовых коэффициентов. Относительная стандартная неопределенность поправочного коэффициента равна 5%.

Ключевые слова: численное моделирование; вычислительные фантомы; ^{90}Sr; красный костный мозг; губчатая кость.

Литература

1. Loke, K.S. Dosimetric Considerations in Radioimmunotherapy and Systemic Radionuclide Therapies: A Review / K.S. Loke, A.K. Padhy, D.C. Ng, A.S. Goh, C. Divgi // World Journal of Nuclear Medicine. – 2011. – V. 10, № 2. – P. 122–138.

2. Дёгтева, М.О. Современное представление о радиоактивном загрязнении реки Теча в 1949-1956 годах / М.О. Дёгтева, Н.Б. Шагина, М.И. Воробьева, Е.А. Шишкина, Е.И. Толстых, А.В. Аклеев // Радиационная биология, радиоэкология. – 2016. – Т. 56, № 5. – С. 523–534.

3. Degteva, M.O. Enhancements in the Techa River Dosimetry System: TRDS-2016D Code for Reconstruction of Deterministic Estimates of Dose from Environmental Exposures / M.O. Degteva, E.I. Tolstykh, E.A. Shishkina, N.B. Shagina, A.Yu. Volchkova, N.G. Bougrov, B.A. Napier, M.A. Smith, L.R. Anspaugh // Health Physics. – 2019. – V. 117, № 4. – P. 378–387.

4. Дёгтева, М.О. Методологический подход к разработке дозиметрических моделей скелета человека для бета-излучающих радионуклидов / М.О. Дёгтева, Е.И. Толстых, Е.А. Шишкина, В.И. Заляпин, П.А. Шарагин, М.А. Смит, Б.А. Напье // Радиационная гигиена. – 2019. – Т. 12, № 2. – С. 66–75.

5. Degteva, M.O. Stochastic Parametric Skeletal Dosimetry Model for Humans: General Approach and Application to Active Marrow Exposure from Bone-Seeking Beta-particle Emitters / M.O. Degteva, E.I. Tolstykh, E.A. Shishkina, P.A. Sharagin, V.I. Zalyapin, A.Yu. Volchkova, M.A. Smith, B.A. Napier // PLos One. – 2021. – V. 16, № 10. – Article ID: e0257605. – 32 p.

6. Shishkina, E.A. Parametric Stochastic Model of Bone Structures to be Used in Computational Dosimetric Phantoms of Human Skeleton / E.A. Shishkina, V.I. Zalyapin, Yu.S. Timofeev, M.O. Degteva, M.A. Smith, B.A. Napier // Radiation and Applications. – 2018. – V. 3, № 2. – P. 133–137.

7. Zalyapin, V.I. Parametric Stochastic Model of Bone Geometry / V.I. Zalyapin, Yu.S. Timofeev, E.A. Shishkina // Вестник ЮУрГУ. Математическое моделирование и программирование. – 2018. – V. 11, № 2. – P. 44–57.

8. Sharagin, P.A. Segmentation of Hematopoietic Sites of Human Skeleton for Calculations of Dose to Active Marrow Exposed to Bone-Seeking Radionuclides / P.A. Sharagin, E.A. Shishkina, E.I. Tolstykh, A.Yu. Volchkova, M.A. Smith, M.O. Degteva // Medical Physics. – 2018. – V. 3. – P. 154–158.

9. Шишкина, Е.А. Аналитическое описание дозообразования в костном мозге от ^{90}Sr, инкорпорированного в кальцифицированных тканях / Е.А. Шишкина, П.А. Шарагин, А.Ю. Волчкова // Вопросы радиационной безопасности. – 2021. – № 3. – С. 72–82.

10. ICRP, 1995. Basic Anatomical and Physiological Data for Use in Radiological Protection – The Skeleton. ICRP Publication 70. Annals of the ICRP. – 1995. – V. 25, № 2. – P. 1–80.

11. Shishkina, E.A. Trabecula: A Random Generator of Computational Phantoms for Bone Marrow Dosimetry / E.A. Shishkina, Yu.S. Timofeev, A.Yu. Volchkova, P.A. Sharagin, V.I. Zalyapin, M.O. Degteva, M.A. Smith, B.A. Napier // Health Physics. – 2020. – V. 118, № 1. – P. 53–59.

12. Шарагин, П.А. Дозиметрическое моделирование кости для остеотропных бета-излучающих радионуклидов: размерные параметры и сегментация / П.А. Шарагин, Е.И. Толстых, Е.А. Шишкина, Б.А. Напье, М.А. Смит, М.О. Дёгтева // Современные проблемы радиобиологии: материалы международной научной конференции. – Минск, 2021. – С. 200–203.

13. Толстых, Е.И. Формирование доз облучения красного костного мозга человека от ^{89,90}Sr, оценка параметров трабекулярной кости для дозиметрического моделирования / Е.И. Толстых, П.А. Шарагин, Е.А. Шишкина, М.О. Дёгтева, Б.А. Напье, М.А. Смит // Современные проблемы радиобиологии: материалы международной научной конференции. – Минск, 2021. – С. 176–179.

14. Soppera, N. JANIS 4: An Improved Version of the NEA Java-Based Nuclear Data Information System / N. Soppera, M. Bossant, E. Dupont // Nuclear Data Sheets. – 2014. – V. 120. – P. 294–296.

Александра Юрьевна Волчкова, кандидат технических наук, научный сотрудник, биофизическая лаборатория, ФГБУН Уральский научно-практический центр радиационной медицины ФМБА России (г. Челябинск, Российская Федерация), alexa_nice2008@mail.ru.

Павел Алексеевич Шарагин, младший научный сотрудник, биофизическая лаборатория, ФГБУН Уральский научно-практический центр радиационной медицины ФМБА России (г. Челябинск, Российская Федерация), pavel.sharagin.1994@gmail.ru.

Елена Анатольевна Шишкина, доктор биологических наук, старший научный сотрудник, биофизическая лаборатория, ФГБУН Уральский научно-практический центр радиационной медицины ФМБА России (г. Челябинск, Российская Федерация); доцент, кафедра радиобиологии, Челябинский государственный университет (г. Челябинск, Российская Федерация), lena@urcrm.ru.

Поступила в редакцию 14 февраля 2022 г.